ACS APPLIED MATERIALS & INTERFACES

www.acsami.org

Research Article

Solution-Processed Isoindigo- and Thienoisoindigo-Based Donor−Acceptor−Donor π-Conjugated Small Molecules: Synthesis, Morphology, Molecular Packing, and Field-Effect Transistor Characterization

Yu-Ting Liao,[▽] Yi-Chun Hsiao,[▽] Yuan-Chih Lo, Chia-Chi Lin, Po-Shen Lin, Shih-Huang Tung, Ken-Tsung Wong,* and Cheng-Liang Liu*

Cite This: *ACS Appl. Mater. Interfaces* 2022, 14, 55886−55897

Read Online

ACCESS | Metrics & More | Article Recommendations | Supporting Information

ABSTRACT: Molecular design and precise control of thin-film morphology and crystallinity of solution-processed small molecules are important for enhancing charge transport mobility of organic field-effect transistors and gaining more insight into the structure−property relationship. Here, two donor−acceptor−donor (D−A−D) architecture small molecules **TRA-IID-TRA** and **TRA-TIID-TRA** comprising an electron-donating triarylamine (**TRA**) and two different electron-withdrawing cores, isoindigo (**IID**) and thienoisoindigo (**TIID**), respectively, were synthesized and characterized. Replacing the phenylene rings of central **IID** A with thiophene gives a **TIID** core, which reduces the optical band gap and upshifts the energy levels of frontier molecular orbitals. The single-crystal structures and grazing-incidence wide-angle X-ray scattering (GIWAXS) analysis revealed that **TRA-TIID-TRA** exhibits the relatively tighter π-π stacking packing with preferential edge-on orientation, larger coherence length, and higher crystallinity due to the noncovalent S···O/S···π intermolecular interactions. The distinctly oriented and connected ribbon-like **TRA-TIID-TRA** crystalline film by the solution-shearing process achieved a superior hole mobility of 0.89 $cm^2 V^{-1} s^{-1}$ in the organic field-effect transistor (OFET) device, which is at least five times higher than that (0.17 $cm^2 V^{-1} s^{-1}$) of **TRA-IID-TRA** with clear cracks. Eventually, rational modulation of fused core in the π-conjugated D−A−D small molecule provides a new understanding of structural design for enhancing the performance of solution-processed organic semiconductors.

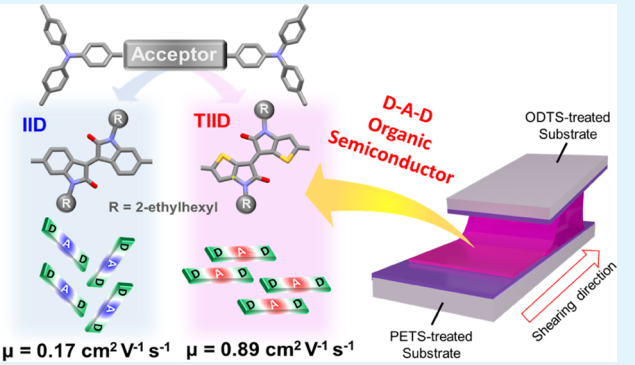

KEYWORDS: *isoindigo, thienoisoindigo, organic transistor, donor−acceptor-donor, triarylamine*

INTRODUCTION

Over the past few decades, the synthesis of π-conjugated semiconductors has received significant attention compared to their inorganic counterparts because of the increasing demand for solution-processed and flexible organic electronics.[1−4] Many efforts have been directed toward the rational molecular design of π-conjugated electroactive and side-chain solubilizing units together with the development of novel processing strategies and device architecture/interface, which demonstrate the significant increase in charge mobility of organic field-effect transistors (OFETs) beyond that of amorphous silicon (0.5−1 $cm^2 V^{-1} s^{-1}$).[5−7] An interesting challenge facing solution-processed organic semiconductors is the complex relationship between the chemical structures, thin-film morphologies, and the resulting electronic properties.[8−15] Therefore, exploring how chromophore structures and processing techniques impact the formation of the organic semiconductor film for order solid-state packing and specific charge transport behavior need to be further investigated.

Organic π-conjugated materials ranging from small molecules to oligomers and polymers used for organic semiconductors usually comprise electron-rich donors (D) and electron-withdrawing acceptors (A) in chromophore-variable chemical architectures and compositions.[16−19] Organic semiconductors using such building blocks can be designed for tunable electronic properties, which potentially contributes to high-performance metrics for several electronic and optoelec-

Received: October 7, 2022
Accepted: December 2, 2022
Published: December 12, 2022

https://doi.org/10.1021/acsami.2c18049
ACS Appl. Mater. Interfaces 2022, 14, 55886−55897

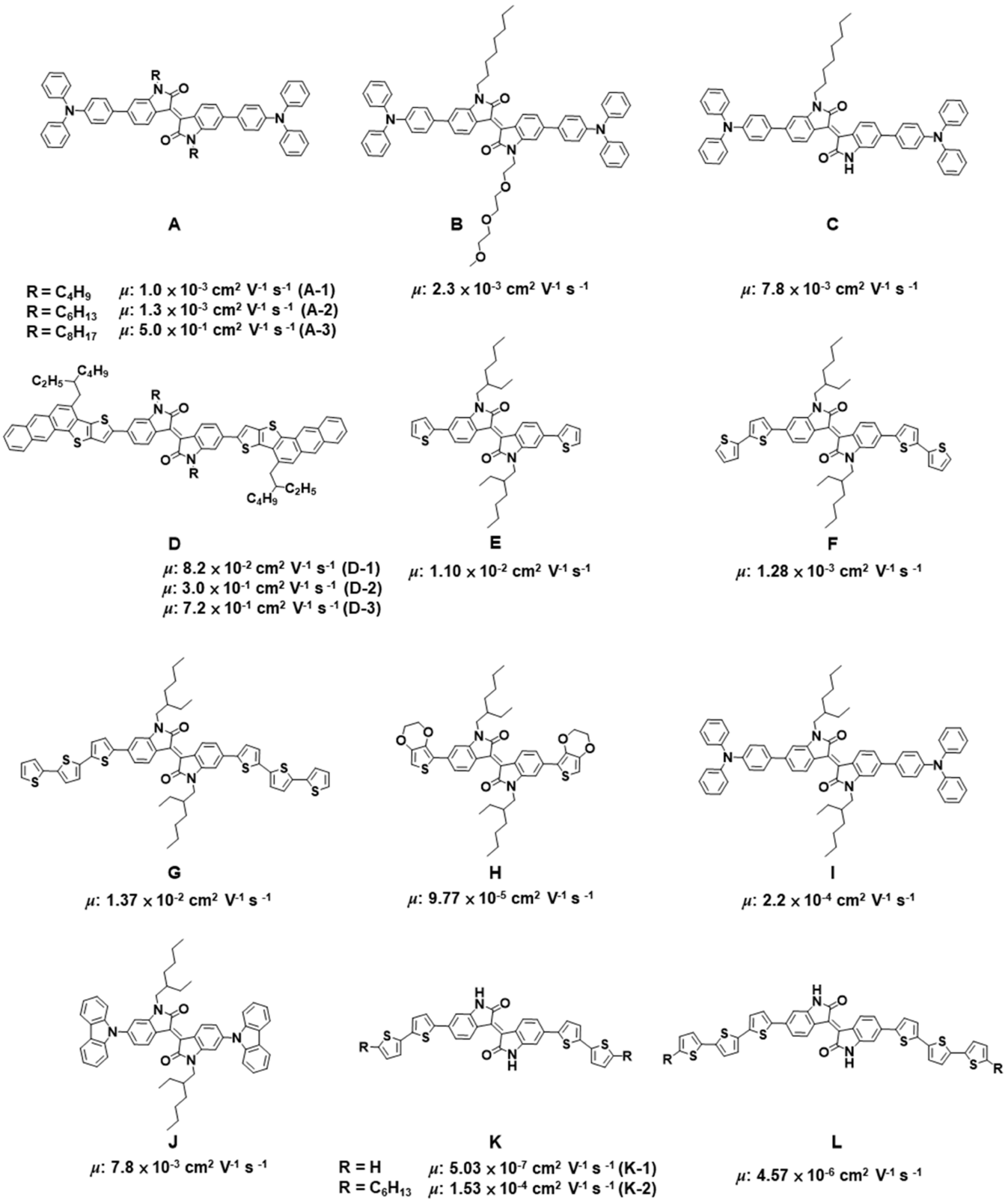

Figure 1. Chemical structures of the reported IID-based D−A−D small-molecule semiconductors: A,[44] B−C,[45] D,[46] E−H,[43] I−J,[47] and K−L.[47] It should be noted that all of the mobilities of semiconductor films reported here are obtained from the spin-coating process.

tronic applications.[20−24] Considering the inherent merits of high purity, batch-to-batch reproducibility, and well-defined molecular structures of small molecules, the D/A unit-derived small molecules were made for the active semiconducting channel of solution-processed OFETs by developing judicious material design strategies,[25,26] especially, the incorporation of electron-withdrawing units as enabling cores is required for semiconducting small molecules.[27−32] Isoindigo (**IID**) electron A with symmetrical lactam architecture is successful for constructing D−A conjugated aromatics and utilizing in

https://doi.org/10.1021/acsami.2c18049
ACS Appl. Mater. Interfaces 2022, 14, 55886−55897

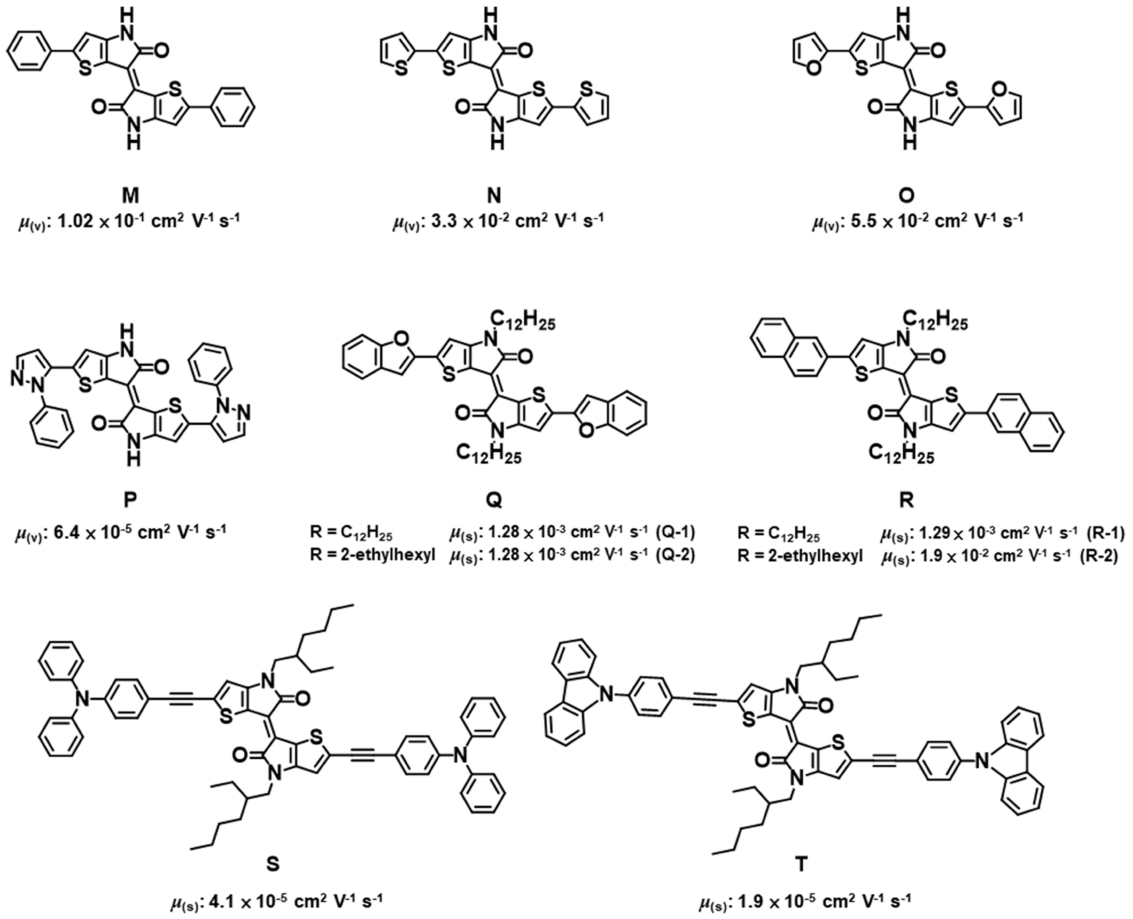

Figure 2. Chemical structures of the reported **TIID**-based small-molecule semiconductors: **M**-**P**,[52] **Q**-**R**,[53,54] and **S**-**T**.[55] The symbols (ν) and (s) denote semiconductor films obtained from the vacuum deposition and spin-coating process, respectively.

Scheme 1. Synthetic Procedure of TRA-TIID-TRA and TRA-IID-TRA Target Organic Semiconductors

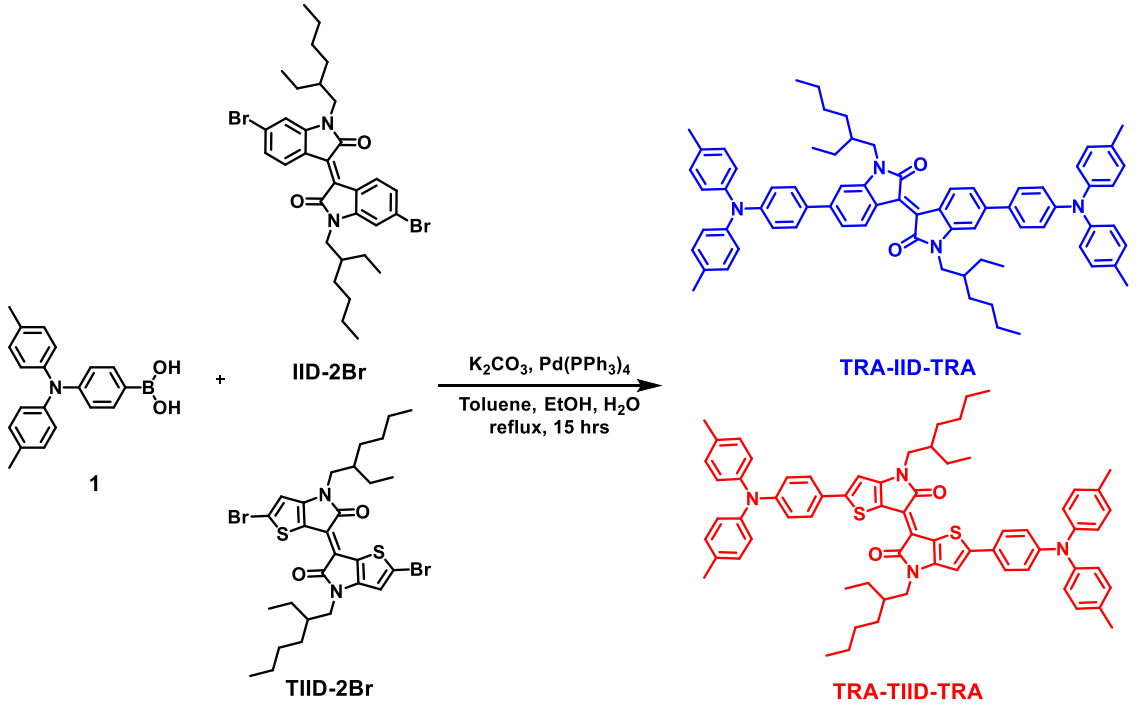

OFET applications due to several combined characteristics of high molecular planarity, extended π-conjugated backbones, strong electron deficiency, and good solubility after alkylation of the amide nitrogen atoms.[33−41] Therefore, molecular

https://doi.org/10.1021/acsami.2c18049
ACS Appl. Mater. Interfaces 2022, 14, 55886−55897

engineering of the **IID** core to extend the conjugated framework with other aromatic motifs in the design of functional small molecules has been attempted.[42−47] In 2010, Reynolds and co-workers first proposed the donor−acceptor−donor (D−A−D) oligomer with **IID** and oligothiophenes as the core and end-capping units, respectively, as a light-harvesting D for molecular bulk heterojunction solar cells.[42] These D−A−D type molecules exhibited a high degree of symmetry architecture for better $\pi-\pi$ stacking intermolecular interactions and reduced reorganization energy, resulting in improved carrier mobility.[48] Subsequently, Lee and co-workers reported a series of **IID**-based D−A−D small molecules with oligothiophenes of variable lengths (compounds **E**−**H** in Figure 1),[43] in which the enhanced mobility of 1.37×10^{-2} cm^2 V^{-1} s^{-1} was observed for compound **G** processed with solvent additive. The chemical structures of reported **IID**-based D−A−D small-molecule semiconductors and their corresponding mobilities are shown in Figure 1. More specifically, core functionalization by replacing the phenylene ring of **IID** with thiophene gives thienoisoindigo (**TIID**) that can improve the molecular planarity due to the oxygen−sulfur (S···O) noncovalent interaction and minimal steric effects of a five-membered heterocyclic ring.[49−51] This thiophene-fused **IID** (**TIID**) possesses a stronger electron-donating ability, thus readily tunable energy levels. The OFET performance of **TIID**-based D−A−D small molecules is also summarized in Figure 2.[52−55] A series of electron Ds were designed as terminal groups for coupling with **TIID** to give new conjugated oligomers with the hole mobilities achieved in the order of $10^{-5}-10^{-2}$ cm^2 V^{-1} s^{-1}. However, the effects of these two isoindigo-based cores (**IID** and **TIID**) on the influence of intermolecular packing structures and charge transport properties of D−A−D small molecules are rarely reported.

Herein, we report the synthesis of two D−A−D p-type semiconducting molecules, **TRA-IID-TRA** and **TRA-TIID-TRA**, as shown in Schemes 1 and S1 (SI), employing heteroisoindigo (**IID** and **TIID**) as the central A and triarylamine (**TRA**) as the capping D together with branched alkyl side chains on the nitrogen of lactam ring to guarantee good solubility. The effects of structural modification on the thermal, optical, electrochemical, and interchain packing and resulting electrical properties were investigated by a comparative study of these two small-molecule semiconductors. **TRA-TIID-TRA** showed a red shift in the absorption and high-lying frontier molecular orbitals, mainly resulting from coplanar geometries and less electron-withdrawing of the **TIID** core. These two compounds displayed preferential edge-on packing structures with varied crystallinity, as confirmed by grazing-incidence wide-angle X-ray scattering (GIWAXS). These different behaviors of heteroisoindigo-based D−A−D small molecules were closely correlated to the electrical characteristics in OFETs. The distinctly oriented and connected ribbon-like **TRA-TIID-TRA** crystalline film achieved by the solution-shearing process exhibits a superior hole mobility of 0.89 cm^2 V^{-1} s^{-1}, which is at least five times higher than that (0.17 cm^2 V^{-1} s^{-1}) of **TRA-IID-TRA** with clear cracks. This result indicates the significant role of the core structure in governing the intermolecular interactions and thus the solid-state electric property.

EXPERIMENTAL SECTION

Synthesis. The synthetic pathways of **TRA-IID-TRA** and **TRA-TIID-TRA** are depicted in Scheme 1. The central core, **IID-2Br**[44] and **TIID-2Br**,[56] reacted with [4-[bis-(4-methylphenyl)amino]-phenyl]boronic acid to give two target organic semiconductors, **TRA-IID-TRA** and **TRA-TIID-TRA**, respectively. The detailed synthetic procedure can be found in the Supporting Information (SI).

Thin-Film Preparation. Both **TRA-IID-TRA** and **TRA-TIID-TRA** solutions were prepared by dissolving the materials in anhydrous 1,2,4-trichlorobenzene (TCB) and chlorobenzene (CB), respectively, warmed to 55 °C. All substrates were cleaned in a sonication bath in acetone and isopropanol, dried under a gentle flow of nitrogen, and cleaned via plasma treatment for 5 min. Solutions were kept at 55 °C before deposition by solution-shearing on the (2-phenylethyl)-trichlorosilane (PETS)-treated SiO_2/Si and Si substrate for OFETs and GIWAXS characterization, respectively, as previously reported.[57−59] Film thickness was controlled by varying concentrations between 4 and 5 mg mL^{-1}, deposition temperature between 90 and 120 °C, a blade speed of 5−45 μm s^{-1}, and a constant gap at 150 μm. The film was prepared under ambient conditions, with post-thermal treatment performed at 150 °C for 15 min inside a nitrogen-filled glovebox. The thickness of **TRA-IID-TRA** and **TRA-TIID-TRA** was determined to be 400 and 100 nm, respectively. The spin-coated films were applied at 2000 rpm for 30 s in a glovebox, followed by the same postannealing condition. The obtained thickness of the spin-coated films is around 60 nm.

Device Fabrication and Characterization. Bottom-gate top-contact device geometries were employed to fabricate the OFETs. A heavily doped Si substrate served as the gate electrode, with a SiO_2 layer (300 nm thick) used as the dielectric. The top source/drain electrodes were deposited onto the solution-sheared organic semiconductors films by thermal evaporation of the Au layer (deposition rate of ~0.5 Å s^{-1}) to give a channel length (L) of 25 nm and a width (W) of 1500 nm. Electrical measurements were performed inside the nitrogen-filled glovebox in the dark using a Keithley 4200-SCS semiconductor characterization system. The field-effect mobility (μ) and threshold voltage (V_{th}) were extracted from the slope and intercept of square root of drain voltage (I_d) versus gate voltage (V_g) curve at the saturation region, according to the following eq 1

$$(I_d)^{1/2} = \frac{W}{2L}\mu\, C_i(V_g - V_{th}) \quad (1)$$

where C_i is the capacitance per unit area of the dielectric layer.

RESULTS AND DISCUSSION

Synthesis and Thermal Properties. Both D−A−D organic semiconductors were prepared via the Suzuki−Miyaura coupling between the two central cores (**IID-2Br** and **TIID-2Br**) and **TRA** end group, as shown in Scheme 1. The methyl groups were introduced onto the terminal positions of the D moiety to block the electroactive site to prevent potential electropolymerization. The chemical structures were fully characterized by mass spectrometry and $^1H/^{13}C$ NMR spectrometry. Both compounds displayed good solubility in common organic solvents, such as toluene, tetrahydrofuran, chloroform, and CB. Figure S1 shows **TRA-IID-TRA** and **TRA-TIID-TRA** well-dissolved in TCB and CB, respectively. Thermal analyses of **TRA-IID-TRA** and **TRA-TIID-TRA** were performed using thermogravimetric analysis (TGA; Figure S2) and differential scanning calorimetry (DSC; Figure S3) under nitrogen conditions. The TGA curves indicated that both compounds exhibit relatively high thermal stability with the high decomposition temperatures (T_d) (corresponding to 5% weight loss) of 343 and 373 °C for **TRA-IID-TRA** and **TRA-TIID-TRA**, respectively. As revealed by the DSC scans, both compounds possess exothermic peaks with sharp exotherms above 220 °C, suggesting strong crystalline behavior.

https://doi.org/10.1021/acsami.2c18049
ACS Appl. Mater. Interfaces 2022, 14, 55886−55897

Optical and Electrochemical Properties. Figure 3 presents the normalized UV−Vis absorption spectra in

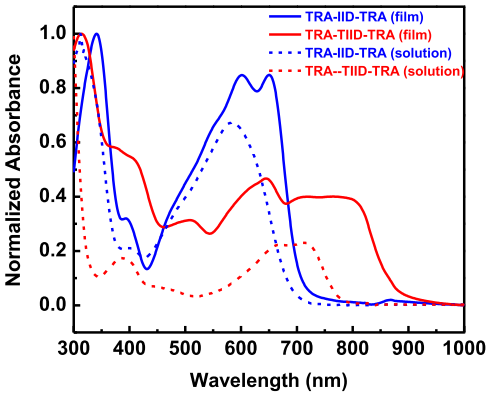

Figure 3. Normalized UV−Vis absorption spectra of **TRA-IID-TRA** in TCB and **TRA-TIID-TRA** CB and their solution-sheared thin films.

solutions and solution-sheared thin films of the two compounds. Both samples in diluted solutions exhibit two main absorption regions: the short- and long-wavelength region (in the range of 300−450 and 450−850 nm) from the $\pi-\pi^*$ transition of **TRA** and **IID**/**TIID** moieties, respectively. Besides, the long-wavelength absorption bands are also associated with the end D-central A intramolecular charge transfer characteristic in addition to the increased conjugation from the flat molecules. Moreover, the corresponding thin-film absorptions are red-shifted and become broader compared with those in the solutions, reflecting considerably increased intermolecular aggregations. The emergence of the vibrational fine structures with these bands in the long-wavelength absorption suggests the presence of some crystallinity in the films. When compared with **TRA-IID-TRA**, the broader region in the main absorption (from 550 to 900 nm) and vibronic features with more red-shifted low-energy absorption maximum and onset in **TRA-TIID-TRA**, which is possibly due to the enhanced degree of planarity from the **TIID** core, results in the extended π-system with powerful molecular interaction.[60] The optical energy band gaps (E_g) were 1.75 and 1.40 eV for **TRA-IID-TRA** and **TRA-TIID-TRA**, respectively, as estimated from thin-film absorption edges (summarized in Table 1). The replacement of phenylene of **IID** with thiophene into **TIID** in the central A moieties gives a smaller band gap. The evidence of molecular orientation of organic semiconductors within the films can be determined by angular-dependent polarized optical spectra, as shown in Figure S4. Both organic semiconductor films show higher optical absorbance when an incident polarized light wave oscillates parallel to the shearing direction ($A_{\parallel}$) and lower in the perpendicular ($A_{\perp}$). The dichroic ratio (DR) described by $A_{\parallel}/A_{\perp}$ is 1.6 and 3.8 for **TRA-IID-TRA** and **TRA-TIID-TRA**, respectively. The higher DR of **TRA-TIID-TRA** indicates that the solution-shearing process helps the orientation of the main chain backbone, and the charge transport properties and anisotropy can be potentially enhanced.[61]

The electrochemical properties of **TRA-IID-TRA** and **TRA-TIID-TRA** were evaluated by cyclic voltammetry, referring to the Fe/Fe^+ redox couple (Figure 4a and Table 1). Reversible oxidation/reduction waves were observed for both compounds presenting good electrochemical stability in cationic/anionic species. The highest occupied molecular orbital/lowest unoccupied molecular orbital (HOMO/LUMO) energy levels were calculated from the oxidation/reduction onset, respectively, and the corresponding energy level diagram is shown in Figure 4b. Compared with **TRA-IID-TRA**, the **TRA-TIID-TRA** presented an up-shifted HOMO and a down-shifted LUMO, which can be ascribed to the more quinoidal and coplanar characteristics of the **TIID** core unit and stronger D−A charge transfer effect.

Molecular Orbital Calculation. The optimization of molecular geometries and the analysis of frontier molecular orbitals (FMOs) at the minima were conducted using density functional theory (DFT) at the B3LYP/6-31G(d) level by the Gaussian 09 program. Figure 5 shows the optimized molecular geometries and the calculated FMOs of these two compounds. The ground-state geometries of these two compounds are both predicted to contain a dihedral angle between the central A and the **TRA** terminal D with the alkyl branched side chain extending out of the molecular plane. However, the replacement of phenylene in **IID** by thiophene in **TIID** enhances the coplanarity between the D and A units (Figure 5a, dihedral angle from 32.8° for **TRA-IID-TRA** to 22.8° for **TRA-TIID-TRA**). The calculated HOMO/LUMO levels are −4.75/−2.63 and −4.33/−2.40 eV for **TRA-IID-TRA** and **TRA-TIID-TRA**, respectively (Figure 5b). These theoretically HOMO/LUMO energy levels vary with the electron A effect in the central core, which are in qualitative agreement with CV data and show that **TRA-TIID-TRA** presents up-shifted HOMO and down-shifted LUMO than **TRA-IID-TRA**, resulting in a smaller HOMO−LUMO energy gap in the isolated state. The effective π-orbital conjugation from less twisted **TRA-TIID-TRA** can explain the reduction in the HOMO−LUMO gap. The molecular orbitals in both compounds show that the HOMO is distributed over the entire π-conjugated framework, as opposed to the LUMO mainly localized on the central A core. It was observed that the electron density in the LUMO wave function of **TRA-TIID-TRA** is slightly delocalized on the side group in the **TRA** D backbones, indicating the lower experimental LUMO energy level of **TRA-TIID-TRA**.

Single-Crystal Structural Analysis. To analyze the effect of the central **IID**/**TIID** core on the single molecular

Table 1. Summary of Thermal, Optical, and Electrochemical Properties

compound	T_d[a] (°C)	T_m[b] (°C)	λ_{max} (sol)[c] (nm)	λ_{max} (film)[d] (nm)	E_g[e] (eV)	E_{ox}[f] (V)	E_{red}[g] (V)	HOMO (eV)	LUMO (eV)
TRA-IID-TRA	343	228	580	602	1.75	0.38	−1.37	−5.18	−3.43
TRA-TIID-TRA	347	264	705	645	1.40	0.12	−1.26	−4.93	−3.54

[a]Decomposition temperature corresponding to 5% weight loss obtained from TGA analysis. [b]Melting temperatures determined from DSC. [c]Obtained in the diluted solution. [d]From the solution-sheared film. [e]Optical band gap estimated from absorption onset of a thin film. [f]Measured in dichloromethane with 0.1 M tetrabutylammonium perchlorate ($TBAPF_6$) as a supporting electrolyte. [g]Measured in THF with 0.1 M tetrabutylammonium perchlorate (TPAP) as a supporting electrolyte.

https://doi.org/10.1021/acsami.2c18049
ACS Appl. Mater. Interfaces 2022, 14, 55886−55897

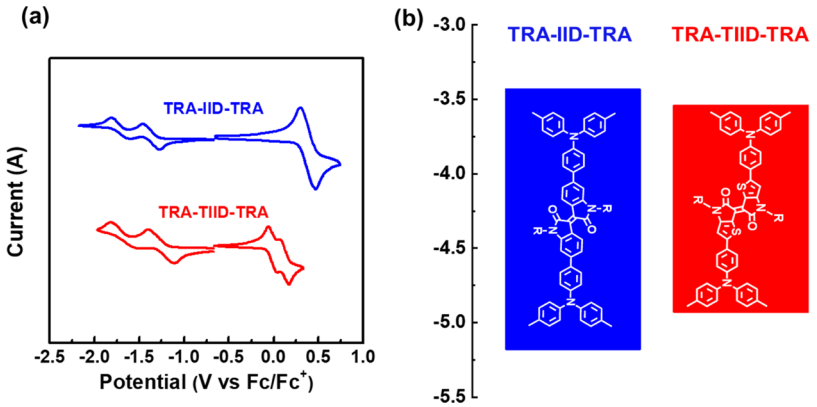

Figure 4. (a) Cyclic voltammograms of **TRA-IID-TRA** and **TRA-TIID-TRA** and (b) their corresponding energy level diagram.

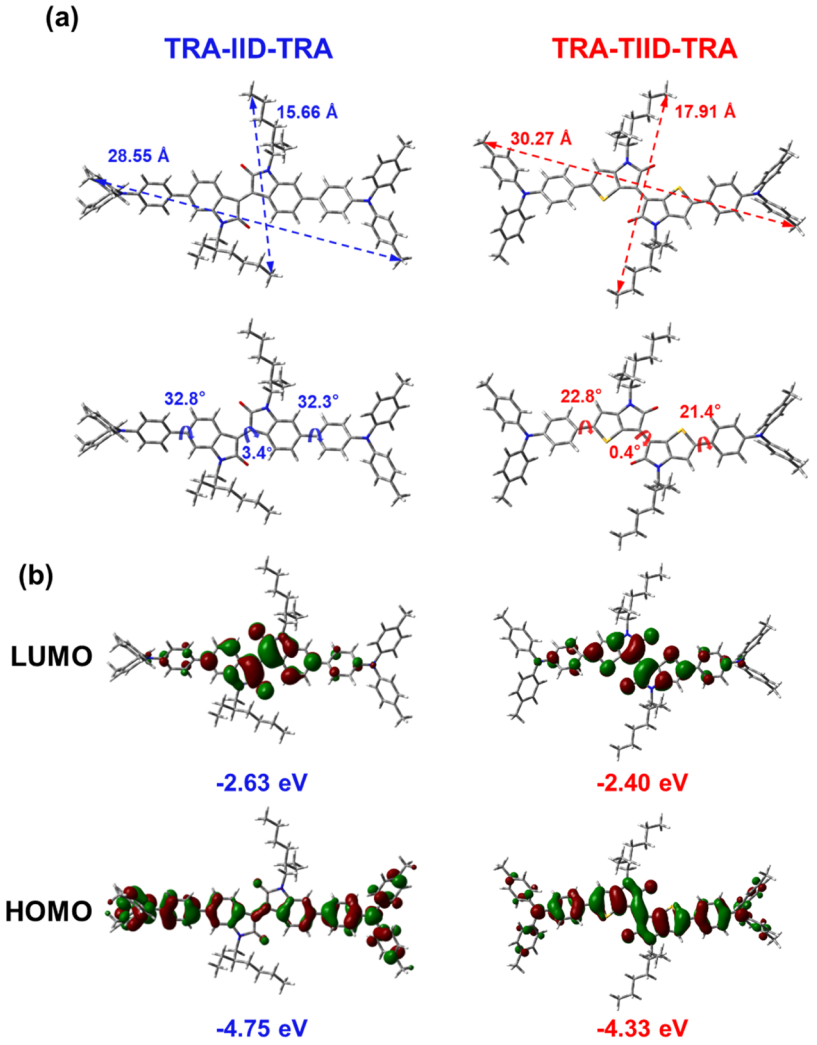

Figure 5. (a) Optimized molecular geometries and measured torsion angle and (b) DFT-derived HOMO and LUMO of **TRA-IID-TRA** and **TRA-TIID-TRA** derivatives.

conformation and intermolecular packing, single-crystal X-ray diffraction (XRD) was performed as shown in Figure 6. Both crystals were obtained from the bilayer solvent (dichloromethane/methanol) diffusion method. **TRA-IID-TRA** molecules adopt a slipped π-stacking pattern, whereas **TRA-TIID-TRA** employs a cofacial and slipped stacking arrangement. Analysis of the single crystal demonstrates that central **IID** and **TIID** units show high core planarity, and the dihedral angles between one part of the A central core and one D terminal are 32.9 and 8.3° for **TRA-IID-TRA** and **TRA-TIID-TRA**, respectively. The relative planar conformation in **TRA-TIID-TRA** may be due to the five-membered thiophene flanked **IID** and the corresponding S···π/S···O interaction. Moreover, the **TRA-TIID-TRA** single crystal (Figure 6b) has a tighter molecular packing than **TRA-IID-TRA** (Figure 6a), with the closest interlayer stacking of 3.96 and 3.61 Å for the former

https://doi.org/10.1021/acsami.2c18049
ACS Appl. Mater. Interfaces 2022, 14, 55886−55897

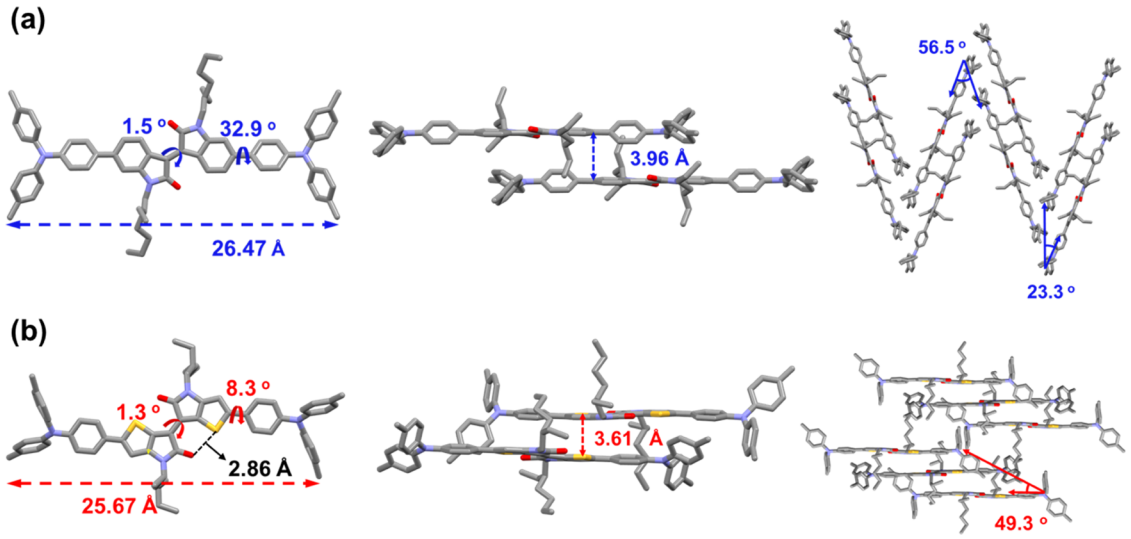

Figure 6. Single-crystal structures in stick models. Top view, front view, and side view of packing of (a) **TRA-IID-TRA** and (b) **TRA-TIID-TRA**.

and latter molecules, respectively, demonstrating a high degree of intermolecular $\pi-\pi$ interaction in **TRA-TIID-TRA**. This suggests a better charge transport pathway within **TRA-TIID-TRA** crystals.

Surface Morphological Properties. The POM images and AFM topographical images of **TRA-IID-TRA** and **TRA-TIID-TRA** thin films are compared in Figure 7. During the

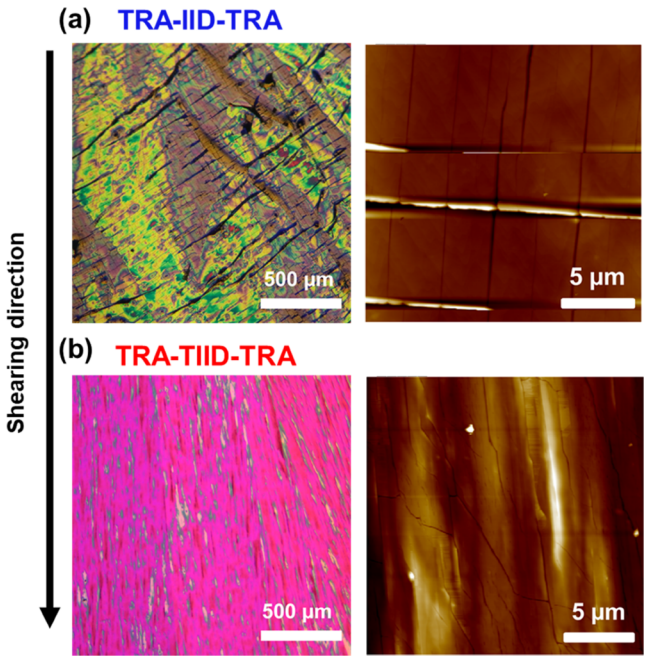

Figure 7. POM and AFM images of solution-sheared (a) **TRA-IID-TRA** and (b) **TRA-TIID-TRA** films.

shearing process, the upper blade drags the top layer of the solution, while the bottom layer adheres to the substrate, which leads to a velocity gradient that causes stress in the solution. The solution becomes saturated upon solvent evaporation, which, along with the stress that orients the molecules, facilitates the nucleation and crystal growth at the meniscus.[62,63] The POM images in Figure 7a display the crystalline structures with a high birefringent and optically anisotropic feature, implying a long-range orientation of **TRA-IID-TRA** and **TRA-TIID-TRA** crystals. Black lines that are roughly perpendicular to the shearing direction can be seen in the **TRA-IID-TRA** film, which are the crack defects generated during the casting process, indicating that **TRA-IID-TRA** is unable to form continuous crystalline domains along the shearing direction. These cracks in **TRA-IID-TRA** may be originated from the more twisted geometry between the propeller shape of end-capped triarylamine and the central **IID** core as well as processing conditions (higher deposition temperature and lower shearing speed). By contrast, the **TRA-TIID-TRA** film shows a significant enhancement in the continuity of oriented connected crystalline domains along the shearing direction, spanning a range in the millimeter scale. Similar surface morphologies were confirmed by AFM analysis (scan area of 20 × 20 μm^2) (Figure 7b). The **TRA-IID-TRA** film shows distinct slits perpendicular to the shear direction, along with small cracks in the shear direction. For the **TRA-TIID-TRA** film, the AFM image reveals continuous domains with only a few wrinkles and tiny cracks. The smoother surface of the **TRA-TIID-TRA** film is reflected by its smaller root-mean-square (RMS) roughness value, 7.8 nm, in comparison to 14.4 nm for **TRA-IID-TRA**. The morphological investigation suggests that the topographically smooth surface of tightly connected and aligned **TRA-TIID-TRA** domains is advantageous to the efficient charge transport across the organic semiconductor films.

Electrical Properties of OFETs. We evaluated the charge transport properties of these two D−A−D organic semiconductors as a function of central cores, according to the field-effect transistor device architecture. Bottom-gate top-contact (BGTC) OFETs were fabricated by shear-depositing organic layers on PETS-modified Si/SiO_2 (300 nm) substrates, and then Au was thermally evaporated as source/drain contacts, as shown in Figure S5. As we discussed earlier, the shear processing during the preparation of the D−A−D small-molecule thin film leads to the in-plane anisotropy of optical and morphological properties with the principal axes parallel and perpendicular to the shearing direction. Therefore, the shearing-induced molecular chain alignment allows the preparation of OFETs with charge transport direction (electrical field) in both directions and to determine the

https://doi.org/10.1021/acsami.2c18049
ACS Appl. Mater. Interfaces 2022, 14, 55886−55897

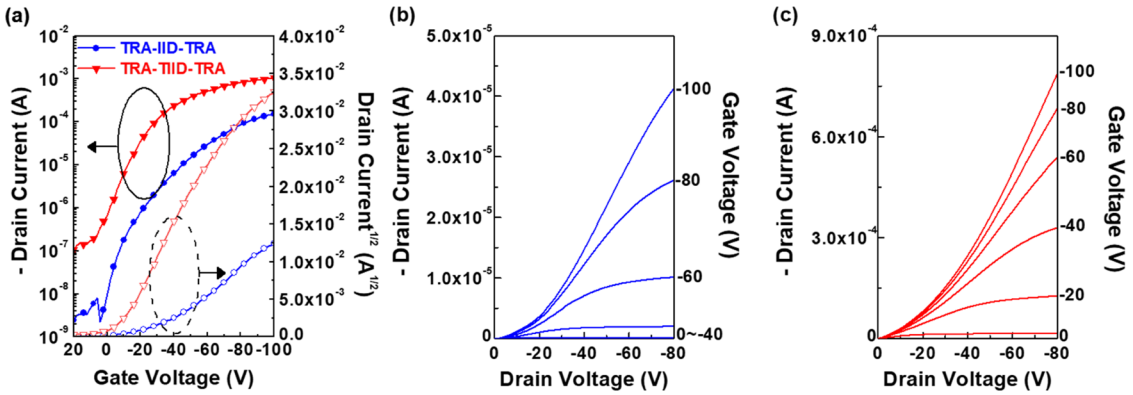

Figure 8. (a) Transfer characteristics for both **TRA-IID-TRA** and **TRA-TIID-TRA** OFETs and output characteristics for (b) **TRA-IID-TRA** and (c) **TRA-TIID-TRA** OFETs, where the charge transport is parallel to the shearing direction.

Table 2. OFET Performance of TRA-IID-TRA and TRA-TIID-TRA

	thin film (∥)[a]				thin film (⊥)[a]			
compound	μ_{max}[b] ($cm^2 V^{-1} s^{-1}$)	μ_{avg}[c] ($cm^2 V^{-1} s^{-1}$)	I_{ON}/I_{OFF}	V_{th} (V)	μ_{max}[b] ($cm^2 V^{-1} s^{-1}$)	μ_{avg}[c] ($cm^2 V^{-1} s^{-1}$)	I_{ON}/I_{OFF}	V_{th} (V)
TRA-IID-TRA	0.17	0.08 ± 0.05	10^4–10^5	20.8 ± 11.8	0.078	0.054 ± 0.002	10^4–10^5	−14.1 ± 12.1
TRA-TIID-TRA	0.89	0.66 ± 0.16	10^3–10^4	−1.7 ± 6.0	0.083	0.043 ± 0.021	10^3–10^4	2.6 ± 5.5

[a]Charge transport direction (source to drain electric field) is symbolized by ∥ (parallel) and ⊥ (perpendicular) to the shearing direction. [b]Maximum mobility. [c]Average mobility.

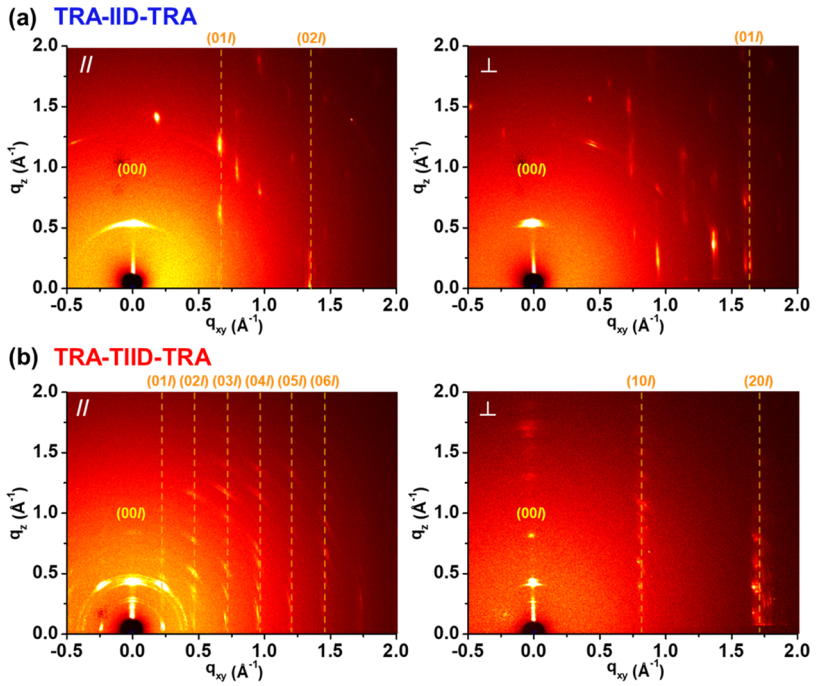

Figure 9. Two-dimensional GIWAXS patterns of (a) **TRA-IID-TRA** and (b) **TRA-TIID-TRA** recorded for the incident X-ray oriented parallel and perpendicular to the shearing direction.

corresponding charge carrier mobilities parallel ($\mu_{\parallel}$)/perpendicular ($\mu_{\perp}$) to the shearing direction. The representative transfer and output curves of **TRA-IID-TRA** and **TRA-TIID-TRA** OFETs with channels parallel and perpendicular to the shearing direction are shown in Figures 8 and S6. The OFET performance parameters extracted from the transfer characteristics are summarized in Table 2, which were explored by analyzing sets of at least 15 device cells for each charge transport direction to reduce the statistical ambiguities. Comparison of the electrical properties of OFET samples was assessed using the saturation region mobility as a figure of merit. All of the OFETs fabricated under both channel directions exhibited the unipolar p-type transport behavior, with mobility in **TRA-TIID-TRA** higher than that of **TRA-IID-TRA**. Only weak hysteresis can be found for the **TRA-TTID-TRA** device upon gate voltage dual sweep due to the good passivation of SiO_2 dielectric (Figure S7). The maximum (average) mobilities of the parallel **TRA-IID-TRA** and **TRA-**

https://doi.org/10.1021/acsami.2c18049
ACS Appl. Mater. Interfaces 2022, 14, 55886−55897

TIID-TRA OFETs were $\mu_{max,\parallel}$ = 0.17 and 0.89 $cm^2\ V^{-1}\ s^{-1}$, while the perpendicular values were $\mu_{max,\perp}$ = 0.078 and 0.083 $cm^2\ V^{-1}\ s^{-1}$, respectively, with a moderately high ON/OFF current ratio (I_{ON}/I_{OFF}) of 10^3-10^5. The **TRA-TIID-TRA**-based OFETs exhibit a μ_{max} enhancement of 5.2× compared to **TRA-IID-TRA**. Deep grain boundaries within the channel of the **TRA-IID-TRA** film are present, which are detrimental to charge transport and reduce mobility. Importantly, a higher I_d was observed when the channel direction was aligned parallel compared to perpendicular at the same V_g. In both organic semiconductor films, $\mu_\parallel$ with the channel along the shearing direction was found to be substantially higher than $\mu_\perp$. The mobility anisotropy ($\mu_\parallel/\mu_\perp$) value of **TRA-IID-TRA** and **TRA-TIID-TRA** was 2.2 and 10.7, respectively. The observed significant difference in mobility values for **TRA-TIID-TRA** films, which correlates with the analysis of polarized absorption results (higher optical DR; Figure S4) also confirm the uniaxial alignment of the solution-sheared **TRA-TIID-TRA**, displaying a strong charge transport anisotropy. The electrical anisotropy found here can also be rationalized in terms of thin-film morphologies since, as observed in the POM images (Figure 7a), when the solution-sheared **TRA-TIID-TRA** thin film exhibits oriented and closely packed crystalline ribbon-like domains. It should be noted that the processing conditions (even post-treatment) significantly influence the crystalline structures.[64] The POM images of solution-sheared **TRA-IID-TRA** and **TRA-TIID-TRA** obtained from various solution-shearing parameters, such as shearing speed and deposition temperature, are shown in Figures S8 and S9, and the corresponding OFET results are summarized in Tables S3 and S4, respectively. The growth of oriented large-sized crystals can be found by optimized solution-shearing parameters to achieve the best device performance reported above. However, the postannealing of the solution-sheared films at elevated temperatures (e.g., 220 °C) does not further improve the OFET performance (summarized in Table S5). Therefore, the solution-sheared films were placed at a specific temperature (150 °C) to remove any residual solvent since the oriented crystals formed under shearing need to be retained for better performance.[65] The understanding of crystallographic directions present in the films correlated to the charge transport properties will be discussed later.

Molecular Packing Analysis. Considering that the microstructures of the semiconducting layer can significantly affect the OFET performance, the molecular stacking, orientation, and crystallinity were further explored by GIWAXS. Figure 9 shows the 2D GIWAXS patterns of the solution-sheared films with the incident beam parallel/perpendicular to the shearing direction. Both films exhibit clear and sharp reflection spots, indicative of a highly crystalline nature and well orientational order in the films. The lamellar packing (00*l*) peaks were stronger in the q_z direction, while the $\pi-\pi$ stacking signals were observed in the q_{xy} direction for these two molecules. This implies that the D−A−D small molecules were predominantly deposited with an edge-on orientation onto the substrate, which may favor the formation of $\pi-\pi$ intermolecular interaction and promote the efficient charge transport in OFETs. The proposed molecular edge-on packing of **TRA-TIID-TRA** crystals is shown in Figure S10. The distinct lamellar peaks are located at 0.50 and 0.39 $Å^{-1}$, corresponding to the spacings of 12.6 and 16.2 Å for **TRA-IID-TRA** and **TRA-TIID-TRA**, respectively, which are the periodical distance between molecular backbones separated by branched alkyls. This lamellar spacing is close to the molecular length along the side chain direction from the theoretical calculation (Figure 5a). Meanwhile, **TRA-IID-TRA** and **TRA-TIID-TRA** display pronounced $\pi-\pi$ diffraction at 1.66 and 1.74 $Å^{-1}$ when the incident beam was perpendicular to the shearing direction, corresponding to the $\pi-\pi$ stacking spacings of 3.79 and 3.60 Å, respectively, which is in line with the results obtained from the single-crystal XRD. It is noteworthy that for **TRA-TIID-TRA** particularly, the (01*l*) peak resulting from the packing along the backbone long axis and the (10*l*) peak from the lateral packing ($\pi-\pi$ stacking) are found for the incident beam parallel and perpendicular to the shearing direction, respectively, manifesting a highly anisotropic alignment caused by the shearing force. This explains the significant difference between $\mu_\parallel$ and $\mu_\perp$ for **TRA-TIID-TRA**. In addition, the crystal coherence length (L_c) that presents the crystallite sizes in the films was determined from the Scherrer equation using the line-cut profiles of the lamellar (001) plane along the q_z direction shown in Figure S11. The L_cs are 314.2 and 448.8 Å for **TRA-IID-TRA** and **TRA-TIID-TRA**, respectively. The larger L_c value of **TRA-TIID-TRA** indicates that this molecule forms larger crystal grains, which is another factor that contributes to the higher charge carrier mobility. These GIWAXS results further demonstrate that the central core in D−A−D molecules could greatly influence the molecular stacking behaviors. Moreover, the effect of the solution-sheared **TRA-IID-TRA** and **TRA-TIID-TRA** under post-thermal annealing treatment at 220 °C is also investigated to monitor the crystallinity, as shown in Figure S12. There is no difference in GIWAXS diffraction patterns for the annealing at regular (150 °C) and higher (220 °C) temperatures. This result agrees with the unchanged data from the postannealing effect with UV−Vis spectra (Figure S13), AFM (Figure S14), POM (Figure S14), and their corresponding charge transport characteristics of semiconducting layers (Table S5).

Finally, the OFET characteristics of the spin-coated films were compared to those processed by the solution-shearing method, as shown in Figure S15. The mobilities obtained from the spin-coated films are 0.0004 and 0.002 $cm^2\ V^{-1}\ s^{-1}$ for **TRA-IID-TRA** and **TRA-TIID-TRA**, respectively (data summarized in Table S6), which are at least two orders of magnitude lower than those of the solution-sheared films. Spin-coated films on the same substrates demonstrate the small crystal (see the POM and AFM images in Figure S16). A few diffuse diffraction patterns in the GIWAXS analysis (Figure S17) suggest a microstructure with a lower degree of structural order kinetically quenched during the spin-coating process. Organic semiconductor films fabricated by solution-shearing enhance the film crystallinity and mobility compared to the isotropic spin-coating process since the aligned crystals provide nucleate sites for the remainder of the compounds in solution and propagate along the shearing direction.[65] The structural design in the central core of D−A−D molecules under the meniscus-assisted shearing process leads to the formation of the ordered structure favorable for a high OFET mobility.

CONCLUSIONS

In summary, solution-processed D−A−D typed small molecules based on **IID** and **TIID** fused central units and an identical electron-donating **TRA** as terminals have been designed, synthesized, and used for the fabrication of OFETs. The effects of the π-conjugated skeleton core on optical and electrochemical properties, thin-film morphology,

https://doi.org/10.1021/acsami.2c18049
ACS Appl. Mater. Interfaces 2022, 14, 55886−55897

molecular crystal packing, and OFET performance were systematically studied. From **TRA-IID-TRA** to **TRA-TIID-TRA** thin films, the absorption spectra red-shifted and frontier molecular orbitals up-shifted. After optimizing the processing condition, the **TRA-TIID-TRA** OFETs delivered a superior hole mobility of 0.89 $cm^2 V^{-1} s^{-1}$, which is significantly higher than that for **TRA-IID-TRA** (0.17 $cm^2 V^{-1} s^{-1}$). The DFT calculation suggested that **TRA-TIID-TRA** shows a more coplanar geometry than **TRA-IID-TRA** due to the presence of the noncovalent interaction. **TRA-TIID-TRA** crystalline thin films showed a more favorable morphology with more compact $\pi-\pi$ stacking, larger coherence length, and a higher degree of crystallinity, which can explain their higher mobility. Our work demonstrates that modulating the hetereocycles in the central fused core by conjugated skeleton strategies provides an effective way to modify the molecular properties of D−A−D small molecules. It is anticipated that various hetereoisoindigo units will be explored to construct such architecture semiconductors to further boost the OFETs' performance.

■ ASSOCIATED CONTENT

Supporting Information

The Supporting Information is available free of charge at https://pubs.acs.org/doi/10.1021/acsami.2c18049.

Synthesis details; instrumentation; ^1H and ^{13}C NMR spectrum; TGA/DSC thermograms; crystal information; polarized UV−Vis absorption; output/transfer plot; proposed molecular packing; and GIWAXS patterns (PDF)

■ AUTHOR INFORMATION

Corresponding Authors

Ken-Tsung Wong − *Department of Chemistry, National Taiwan University, Taipei 10617, Taiwan; Institute of Atomic and Molecular Science, Academia Sinica, Taipei 10617, Taiwan;* orcid.org/0000-0002-1680-6186; Email: kenwong@ntu.edu.tw

Cheng-Liang Liu − *Department of Materials Science and Engineering, National Taiwan University, Taipei 10617, Taiwan;* orcid.org/0000-0002-8778-5386; Email: liucl@ntu.edu.tw

Authors

Yu-Ting Liao − *Department of Chemistry, National Taiwan University, Taipei 10617, Taiwan*

Yi-Chun Hsiao − *Department of Materials Science and Engineering, National Taiwan University, Taipei 10617, Taiwan*

Yuan-Chih Lo − *Department of Chemistry, National Taiwan University, Taipei 10617, Taiwan*

Chia-Chi Lin − *Department of Chemical and Materials Engineering, National Central University, Taoyuan 32001, Taiwan*

Po-Shen Lin − *Department of Materials Science and Engineering, National Taiwan University, Taipei 10617, Taiwan*

Shih-Huang Tung − *Institute of Polymer Science and Engineering, National Taiwan University, Taipei 10617, Taiwan;* orcid.org/0000-0002-6787-4955

Complete contact information is available at: https://pubs.acs.org/10.1021/acsami.2c18049

Author Contributions

$^{\nabla}$Y.-T.L. and Y.-C.H. contributed equally. This manuscript was written through contributions of all authors. All authors have given approval to the final version of the manuscript.

Notes

The authors declare no competing financial interest.

■ ACKNOWLEDGMENTS

K.-T.W. thanks the financial support from the National Science and Technology Council (NSTC) in Taiwan (110-2113-M-002-008-MY3). C.-L.L. gratefully acknowledges the funding from the Young Scholar Fellowship Program (Columbus Program) and 2030 Cross-Generation Young Scholars Program by NSTC in Taiwan, under Grant 110-2636-E-002-021 and 111-2628-E-002-014, respectively. The authors thank Beamline B13A1/B17A1/B23A1 from the National Synchrotron Radiation Research Center (NSRRC) of Taiwan for providing beamtime.

■ REFERENCES

(1) Kumagai, S.; Ishii, H.; Watanabe, G.; Yu, C. P.; Watanabe, S.; Takeya, J.; Okamoto, T. Nitrogen-Containing Perylene Diimides: Molecular Design, Robust Aggregated Structures, and Advances in N-Type Organic Semiconductors. *Acc. Chem. Res.* **2022**, *55*, 660−672.

(2) Liu, K.; Ouyang, B.; Guo, X.; Guo, Y.; Liu, Y. Advances in Flexible Organic Field-Effect Transistors and Their Applications for Flexible Electronics. *npj Flex. Electron.* **2022**, *6*, No. 1.

(3) Irimia-Vladu, M.; Kanbur, Y.; Camaioni, F.; Coppola, M. E.; Yumusak, C.; Irimia, C. V.; Vlad, A.; Operamolla, A.; Farinola, G. M.; Suranna, G. P.; González-Benitez, N.; Molina, M. C.; Bautista, L. F.; Langhals, H.; Stadlober, B.; Głowacki, E. D.; Sariciftci, N. S. Stability of Selected Hydrogen Bonded Semiconductors in Organic Electronic Devices. *Chem. Mater.* **2019**, *31*, 6315−6346.

(4) Sun, Y.; Guo, Y.; Liu, Y. Design and Synthesis of High Performance Π-Conjugated Materials through Antiaromaticity and Quinoid Strategy for Organic Field-Effect Transistors. *Mater. Sci. Eng., R* **2019**, *136*, 13−26.

(5) Yao, Z.-F.; Wang, J.-Y.; Pei, J. High-Performance Polymer Field-Effect Transistors: From the Perspective of Multi-Level Microstructures. *Chem. Sci.* **2021**, *12*, 1193−1205.

(6) Chen, H.; Zhang, W.; Li, M.; He, G.; Guo, X. Interface Engineering in Organic Field-Effect Transistors: Principles, Applications, and Perspectives. *Chem. Rev.* **2020**, *120*, 2879−2949.

(7) Kim, D.; Kim, F. S. Materials Chemistry, Device Engineering, and Promising Applications of Polymer Transistors. *Chem. Mater.* **2021**, *33*, 7572−7594.

(8) Nguyen, N. N.; Lee, H.; Lee, H. C.; Cho, K. Van Der Waals Epitaxy of Organic Semiconductor Thin Films on Atomically Thin Graphene Templates for Optoelectronic Applications. *Acc. Chem. Res.* **2022**, *55*, 673−684.

(9) Okamoto, T.; Yu, C. P.; Mitsui, C.; Yamagishi, M.; Ishii, H.; Takeya, J. Bent-Shaped P-Type Small-Molecule Organic Semiconductors: A Molecular Design Strategy for Next-Generation Practical Applications. *J. Am. Chem. Soc.* **2020**, *142*, 9083−9096.

(10) Huang, J.; Yu, G. Structural Engineering in Polymer Semiconductors with Aromatic N-Heterocycles. *Chem. Mater.* **2021**, *33*, 1513−1539.

(11) Callaway, C. P.; Liu, A. L.; Venkatesh, R.; Zheng, Y.; Lee, M.; Meredith, J. C.; Grover, M.; Risko, C.; Reichmanis, E. The Solution Is the Solution: Data-Driven Elucidation of Solution-to-Device Feature Transfer for Π-Conjugated Polymer Semiconductors. *ACS Appl. Mater. Interfaces* **2022**, *14*, 3613−3620.

(12) Fratini, S.; Nikolka, M.; Salleo, A.; Schweicher, G.; Sirringhaus, H. Charge Transport in High-Mobility Conjugated Polymers and Molecular Semiconductors. *Nat. Mater.* **2020**, *19*, 491−502.

(13) Huang, H.; Yang, L.; Facchetti, A.; Marks, T. J. Organic and Polymeric Semiconductors Enhanced by Noncovalent Conformational Locks. *Chem. Rev.* **2017**, *117*, 10291−10318.
(14) Khim, D.; Luzio, A.; Bonacchini, G. E.; Pace, G.; Lee, M. J.; Noh, Y. Y.; Caironi, M. Uniaxial Alignment of Conjugated Polymer Films for High-Performance Organic Field-Effect Transistors. *Adv. Mater.* **2018**, *30*, No. 1705463.
(15) Chung, H.; Diao, Y. Polymorphism as an Emerging Design Strategy for High Performance Organic Electronics. *J. Mater. Chem. C* **2016**, *4*, 3915−3933.
(16) Wu, J. S.; Cheng, S. W.; Cheng, Y. J.; Hsu, C. S. Donor-Acceptor Conjugated Polymers Based on Multifused Ladder-Type Arenes for Organic Solar Cells. *Chem. Soc. Rev.* **2015**, *44*, 1113−1154.
(17) Zhang, J.; Xu, W.; Sheng, P.; Zhao, G. Y.; Zhu, D. B. Organic Donor-Acceptor Complexes as Novel Organic Semiconductors. *Acc. Chem. Res.* **2017**, *50*, 1654−1662.
(18) Kim, M.; Ryu, S. U.; Park, S. A.; Choi, K.; Kim, T.; Chung, D.; Park, T. Donor-Acceptor-Conjugated Polymer for High-Performance Organic Field-Effect Transistors: A Progress Report. *Adv. Funct. Mater.* **2020**, *30*, No. 1904545.
(19) Liu, Q.; Bottle, S. E.; Sonar, P. Developments of Diketopyrrolopyrrole-Dye-Based Organic Semiconductors for a Wide Range of Applications in Electronics. *Adv. Mater.* **2020**, *32*, No. 1903882.
(20) Huang, Y.; Elder, D. L.; Kwiram, A. L.; Jenekhe, S. A.; Jen, A. K. Y.; Dalton, L. R.; Luscombe, C. K. Organic Semiconductors at the University of Washington: Advancements in Materials Design and Synthesis and toward Industrial Scale Production. *Adv. Mater.* **2021**, *33*, No. 1904239.
(21) Jiang, H.; Hu, W. P. The Emergence of Organic Single-Crystal Electronics. *Angew. Chem. Int. Ed.* **2020**, *59*, 1408−1428.
(22) Lee, C.; Lee, S.; Kim, G. U.; Lee, W.; Kim, B. J. Recent Advances, Design Guidelines, and Prospects of All-Polymer Solar Cells. *Chem. Rev.* **2019**, *119*, 8028−8086.
(23) Zhang, J.; Jin, J. Q.; Xu, H. X.; Zhang, Q. C.; Huang, W. Recent Progress on Organic Donor-Acceptor Complexes as Active Elements in Organic Field-Effect Transistors. *J. Mater. Chem. C* **2018**, *6*, 3485−3498.
(24) Lee, E. K.; Lee, M. Y.; Park, C. H.; Lee, H. R.; Oh, J. H. Toward Environmentally Robust Organic Electronics: Approaches and Applications. *Adv. Mater.* **2017**, *29*, No. 1703638.
(25) Wang, Y.; Sun, L.; Wang, C.; Yang, F.; Ren, X.; Zhang, X.; Dong, H.; Hu, W. Organic Crystalline Materials in Flexible Electronics. *Chem. Soc. Rev.* **2019**, *48*, 1492−1530.
(26) Yu, L. Y.; Portale, G.; Stingelin, N. Solution-Processing of Semiconducting Organic Small Molecules: What We Have Learnt from 5,11-Bis(Triethylsilylethynyl)Anthradithiophene. *J. Mater. Chem. C* **2021**, *9*, 10547−10556.
(27) Feng, K.; Guo, H.; Sun, H.; Guo, X. N-Type Organic and Polymeric Semiconductors Based on Bithiophene Imide Derivatives. *Acc. Chem. Res.* **2021**, *54*, 3804−3817.
(28) Zhang, C.; Zhu, X. N-Type Quinoidal Oligothiophene-Based Semiconductors for Thin-Film Transistors and Thermoelectrics. *Adv. Funct. Mater.* **2020**, *30*, No. 2000765.
(29) Sun, H.; Guo, X.; Facchetti, A. High-Performance N-Type Polymer Semiconductors: Applications, Recent Development, and Challenges. *Chem* **2020**, *6*, 1310−1326.
(30) Ren, Y.; Yang, X. Y.; Zhou, L.; Mao, J. Y.; Han, S. T.; Zhou, Y. Recent Advances in Ambipolar Transistors for Functional Applications. *Adv. Funct. Mater.* **2019**, *29*, No. 1902105.
(31) Wang, Y.; Michinobu, T. Rational Design Strategies for Electron-Deficient Semiconducting Polymers in Ambipolar/N-Channel Organic Transistors and All-Polymer Solar Cells. *J. Mater. Chem. C* **2018**, *6*, 10390−10410.
(32) Quinn, J. T. E.; Zhu, J. X.; Li, X.; Wang, J. L.; Li, Y. N. Recent Progress in the Development of N-Type Organic Semiconductors for Organic Field Effect Transistors. *J. Mater. Chem. C* **2017**, *5*, 8654−8681.
(33) Wei, X.; Zhang, W.; Yu, G. Semiconducting Polymers Based on Isoindigo and Its Derivatives: Synthetic Tactics, Structural Modifications, and Applications. *Adv. Funct. Mater.* **2021**, *31*, No. 2010979.
(34) Wang, E. G.; Mammo, W.; Andersson, M. R. 25th Anniversary Article: Isoindigo- Based Polymers and Small Molecules for Bulk Heterojunction Solar Cells and Field Effect Transistors. *Adv. Mater.* **2014**, *26*, 1801−1826.
(35) Zhou, Y. K.; Zhang, W. F.; Yu, G. Recent Structural Evolution of Lactam- and Imide-Functionalized Polymers Applied in Organic Field-Effect Transistors and Organic Solar Cells. *Chem. Sci.* **2021**, *12*, 6844−6878.
(36) Li, J. L.; Cao, J. J.; Duan, L. L.; Zhang, H. L. Evolution of Isoindigo-Based Electron-Deficient Units for Organic Electronics: From Natural Dyes to Organic Semiconductors. *Asian J. Org. Chem.* **2018**, *7*, 2147−2160.
(37) Gsänger, M.; Bialas, D.; Huang, L. Z.; Stolte, M.; Wurthner, F. Organic Semiconductors Based on Dyes and Color Pigments. *Adv. Mater.* **2016**, *28*, 3615−3645.
(38) Lei, T.; Wang, J. Y.; Pei, J. Design, Synthesis, and Structure-Property Relationships of Isoindigo-Based Conjugated Polymers. *Acc. Chem. Res.* **2014**, *47*, 1117−1126.
(39) Wang, Y. Z.; Yu, Y. P.; Liao, H. L.; Zhou, Y. C.; McCulloch, I.; Yue, W. The Chemistry and Applications of Heteroisoindigo Units as Enabling Links for Semiconducting Materials. *Acc. Chem. Res.* **2020**, *53*, 2855−2868.
(40) Park, K. H.; Go, J. Y.; Lim, B.; Noh, Y. Y. Recent Progress in Lactam-Based Polymer Semiconductors for Organic Electronic Devices. *J. Polym. Sci.* **2022**, *60*, 429−485.
(41) Deng, P.; Zhang, Q. Recent Developments on Isoindigo-Based Conjugated Polymers. *Polym. Chem.* **2014**, *5*, 3298−3305.
(42) Mei, J.; Graham, K. R.; Stalder, R.; Reynolds, J. R. Synthesis of Isoindigo-Based Oligothiophenes for Molecular Bulk Heterojunction Solar Cells. *Org. Lett.* **2010**, *12*, 660−663.
(43) Park, Y. J.; Seo, J. H.; Elsawy, W.; Walker, B.; Cho, S.; Lee, J.-S. Enhanced Performance in Isoindigo Based Organic Small Molecule Field-Effect Transistors through Solvent Additives. *J. Mater. Chem. C* **2015**, *3*, 5951−5957.
(44) Dharmapurikar, S. S.; Arulkashmir, A.; Das, C.; Muddellu, P.; Krishnamoorthy, K. Enhanced Hole Carrier Transport Due to Increased Intermolecular Contacts in Small Molecule Based Field Effect Transistors. *ACS Appl. Mater. Interfaces* **2013**, *5*, 7086−7093.
(45) Dharmapurikar, S. S.; Arul Kashmir, A.; Kumari, T.; Kalalawe, V.; Kanetkar, M.; Chini, M. K. Significance of Secondary Forces toward Improving the Charge Carrier Mobility of Isoindigo Based Conjugated Small Molecules. *Chem. Phys. Lett.* **2021**, *774*, No. 138621.
(46) Shao, J.; Zhang, X.; Tian, H.; Geng, Y.; Wang, F. Donor−Acceptor−Donor Conjugated Oligomers Based on Isoindigo and Anthra[1,2-B]Thieno[2,3-D]Thiophene for Organic Thin-Film Transistors: The Effect of the Alkyl Side Chain Length on Semiconducting Properties. *J. Mater. Chem. C* **2015**, *3*, 7567−7574.
(47) Patil, H.; Chang, J.; Gupta, A.; Bilic, A.; Wu, J.; Sonar, P.; Bhosale, S. V. Isoindigo-Based Small Molecules with Varied Donor Components for Solution-Processable Organic Field Effect Transistor Devices. *Molecules* **2015**, *20*, 17362−17377.
(48) Pham, H. D.; Jain, S. M.; Li, M.; Wang, Z.-K.; Manzhos, S.; Feron, K.; Pitchaimuthu, S.; Liu, Z.; Motta, N.; Durrant, J. R.; Sonar, P. All-Rounder Low-Cost Dopant-Free D-a-D Hole-Transporting Materials for Efficient Indoor and Outdoor Performance of Perovskite Solar Cells. *Adv. Electron. Mater.* **2020**, *6*, No. 1900884.
(49) Odajima, T.; Ashizawa, M.; Konosu, Y.; Matsumoto, H.; Mori, T. The Impact of Molecular Planarity on Electronic Devices in Thienoisoindigo-Based Organic Semiconductors. *J. Mater. Chem. C* **2014**, *2*, 10455−10467.
(50) Yoo, D.; Hasegawa, T.; Ashizawa, M.; Kawamoto, T.; Masunaga, H.; Hikima, T.; Matsumoto, H.; Mori, T. N-Unsubstituted Thienoisoindigos: Preparation, Molecular Packing and Ambipolar

https://doi.org/10.1021/acsami.2c18049
ACS Appl. Mater. Interfaces 2022, 14, 55886−55897

Organic Field-Effect Transistors. *J. Mater. Chem. C* **2017**, *5*, 2509−2512.
(51) Hasegawa, T.; Ashizawa, M.; Matsumoto, H. Design and Structure−Property Relationship of Benzothienoisoindigo in Organic Field Effect Transistors. *RSC Adv.* **2015**, *5*, 61035−61043.
(52) Yoo, D.; Hasegawa, T.; Kohara, A.; Sugiyama, H.; Ashizawa, M.; Kawamoto, T.; Masunaga, H.; Hikima, T.; Ohta, N.; Uekusa, H.; Matsumoto, H.; Mori, T. Ambipolar Organic Field-Effect Transistors Based on N-Unsubstituted Thienoisoindigo Derivatives. *Dyes Pigm.* **2020**, *180*, No. 108418.
(53) Han, P.; Gong, X.; Lin, B.; Jia, Z.; Ye, S.; Sun, Y.; Yang, H. Solution Processable Low Bandgap Thienoisoindigo-Based Small Molecules for Organic Electronic Devices. *RSC Adv.* **2015**, *5*, 50098−50104.
(54) Nketia-Yawson, B.; Kang, H.; Shin, E.-Y.; Xu, Y.; Yang, C.; Noh, Y.-Y. Effect of Electron-Donating Unit on Crystallinity and Charge Transport in Organic Field-Effect Transistors with Thienoisoindigo-Based Small Molecules. *Org. Electron.* **2015**, *26*, 151−157.
(55) Vybornyi, O.; Jiang, Y.; Baert, F.; Demeter, D.; Roncali, J.; Blanchard, P.; Cabanetos, C. Solution-Processable Thienoisoindigo-Based Molecular Donors for Organic Solar Cells with High Open-Circuit Voltage. *Dyes Pigm.* **2015**, *115*, 17−22.
(56) Wang, B.-C.; Tai, C.-K.; Chou, P.-T.; Hsu, Y.-T.; Chen, L.; Liu, C.-K.; Chan, L.-H.; Chen, C.-H. Novel Thienoisoindigo-Based Dyes for near-Infrared Organic Photovoltaics - a Combination of Theoretical and Experimental Study. *Org. Electron.* **2017**, *51*, 410−421.
(57) Vegiraju, S.; Chang, B.-C.; Priyanka, P.; Huang, D.-Y.; Wu, K.-Y.; Li, L.-H.; Chang, W.-C.; Lai, Y.-Y.; Hong, S.-H.; Yu, B.-C.; Wang, C.-L.; Chang, W.-J.; Liu, C.-L.; Chen, M.-C.; Facchetti, A. Intramolecular Locked Dithioalkylbithiophene-Based Semiconductors for High-Performance Organic Field-Effect Transistors. *Adv. Mater.* **2017**, *29*, No. 1702414.
(58) Vegiraju, S.; He, G.-Y.; Kim, C.; Priyanka, P.; Chiu, Y.-J.; Liu, C.-W.; Huang, C.-Y.; Ni, J.-S.; Wu, Y.-W.; Chen, Z.; Lee, G.-H.; Tung, S.-H.; Liu, C.-L.; Chen, M.-C.; Facchetti, A. Solution-Processable Dithienothiophenoquinoid (Dttq) Structures for Ambient-Stable N-Channel Organic Field Effect Transistors. *Adv. Funct. Mater.* **2017**, *27*, No. 1606761.
(59) Vegiraju, S.; Amelenan Torimtubun, A. A.; Lin, P.-S.; Tsai, H.-C.; Lien, W.-C.; Chen, C.-S.; He, G.-Y.; Lin, C.-Y.; Zheng, D.; Huang, Y.-F.; Wu, Y.-C.; Yau, S.-L.; Lee, G.-H.; Tung, S.-H.; Wang, C.-L.; Liu, C.-L.; Chen, M.-C.; Facchetti, A. Solution-Processable Quinoidal Dithioalkylterthiophene-Based Small Molecules Pseudo-Pentathienoacenes Via an Intramolecular S···S Lock for High-Performance N-Type Organic Field-Effect Transistors. *ACS Appl. Mater. Interfaces* **2020**, *12*, 25081−25091.
(60) Lu, C.; Chen, H.-C.; Chuang, W.-T.; Hsu, Y.-H.; Chen, W.-C.; Chou, P.-T. Interplay of Molecular Orientation, Film Formation, and Optoelectronic Properties on Isoindigo- and Thienoisoindigo-Based Copolymers for Organic Field Effect Transistor and Organic Photovoltaic Applications. *Chem. Mater.* **2015**, *27*, 6837−6847.
(61) Pandey, M.; Kumari, N.; Nagamatsu, S.; Pandey, S. S. Recent Advances in the Orientation of Conjugated Polymers for Organic Field-Effect Transistors. *J. Mater. Chem. C* **2019**, *7*, 13323−13351.
(62) Gu, X.; Shaw, L.; Gu, K.; Toney, M. F.; Bao, Z. The Meniscus-Guided Deposition of Semiconducting Polymers. *Nat. Commun.* **2018**, *9*, No. 534.
(63) Lu, Z. J.; Wang, C. Q.; Deng, W.; Achille, M. T.; Jie, J. S.; Zhang, X. J. Meniscus-Guided Coating of Organic Crystalline Thin Films for High-Performance Organic Field-Effect Transistors. *J. Mater. Chem. C* **2020**, *8*, 9133−9146.
(64) Chen, M.; Peng, B.; Huang, S.; Chan, P. K. L. Understanding the Meniscus-Guided Coating Parameters in Organic Field-Effect-Transistor Fabrications. *Adv. Funct. Mater.* **2020**, *30*, No. 1905963.
(65) Becerril, H. A.; Roberts, M. E.; Liu, Z.; Locklin, J.; Bao, Z. High-Performance Organic Thin-Film Transistors through Solution-Sheared Deposition of Small-Molecule Organic Semiconductors. *Adv. Mater.* **2008**, *20*, 2588−2594.

https://doi.org/10.1021/acsami.2c18049
ACS Appl. Mater. Interfaces 2022, 14, 55886−55897